



## The Ballistic Behavior of High Strength, Low Alloy-100 Steel at Sub-zero Temperatures

G. Majzoobi\*, S. Moradi

Mechanical Engineering Department, Bu-Ali Sina University, Hamedan, Iran

### PAPER INFO

#### Paper history:

Received 29 December 2015

Received in revised form 29 September 2016

Accepted 30 September 2016

#### Keywords:

High Strength, Low Alloy -100

Ballistic Limit

Sub-zero Temperature

Lambert-Jonas

Residual Velocity

### ABSTRACT

The ballistic response of the high strength, low alloy (HSLA-100) steel at ambient and temperatures of -40, -80 and -196°C is investigated in this work. Lambert-jonas equation is used to fit the experimental results into a curve. The effect of quenching on ballistic behavior of HSLA-100 is also studied. The experiments are conducted on 3mm thick rectangular specimens impacted by blunt tip projectiles. The results indicate that for the as-received material, the ballistic limit is nearly the same for ambient and -40°C temperatures, but increases significantly by 30% and 40% for -80 and -196°C temperatures, respectively. The same trend is observed for the quenched specimens. However, the increase of ballistic limit is lower for the quenched specimens and is 16% and 30% for -80 and -196°C temperatures, respectively. The ballistic test was also simulated using Ls-dyna hydrocode to examine the effect of parameters such as the specimen's thickness, the projectile's tip shape and mass on the ballistic limit of the materials.

doi: 10.5829/idosi.ije.2016.29.12c.14

## 1. INTRODUCTION

High strength low alloy (HSLA) steels constitute an important class of steels estimated to be around 12% of total world steel production. Due to its high strength, toughness and weldability, HSLA steels are widely used in structural applications such as naval vessels, buildings, canes, power transportation, gas and petrol pipes, agricultural machineries, ships and submarines [1-4]. The objective of the HSLA-100 steel production was a bainitic matrix which enjoys a good combination of the strength and toughness properties [5]. Over the past recent years, a number of studies have been accomplished on HSLA steels but these studies are mostly related to quasi-static and fatigue loadings and the strength of welded connections made of this type of alloys [6, 7]. There are foot prints in the literature of studies on the dynamic behavior of HSLA steels [8, 9]. The effect of heat treatment on microstructure and the properties of high strength low carbon steels have also been investigated [10-13]. In general, the properties of

HSLA alloys have been the subject of many investigations over the past several decades. These investigations have mainly focused on microstructural examinations, mechanical characterization and metallurgical aspects of HSLA under various loading and environmental conditions. However, less attention has been paid to the ballistic behavior of the material particularly under frigorific conditions. Martineau et al. [14] investigated the penetration of Tungsten projectiles into the plate targets made of HSLA-100 alloys within the range of velocities 800 to 2500 m/sec. In the present study, the ballistic behavior of HSLA-100 steels was investigated at ambient and subzero temperatures of -40, -80 and -196 °C. The ballistic limit of the alloy could be estimated using the semi empirical or analytical models such as Lambert-Jonas [15] and Recht-Ipson [16] models. Both models are based on the conservation of momentum principal defined by:

$$\frac{1}{2} m_i v_i^2 = \frac{1}{2} m_r v_r^2 + \Sigma E \quad (1)$$

where,  $v_i$  and  $v_r$  are the impact and residual velocities, respectively. Recht-Ipson model is usually used for the

\*Corresponding Author's Email: gh\_majzoobi@yahoo.co.uk (G. Majzoobi)

cases when a rigid projectile hits a thin target in a normal direction. Lambert-Jonas model can be used for oblique impact on thick targets and considers the errors due to test conditions. In Recht-Ipson model we have:

$$v_i^2 = v_r^2 + v_{50}^2 \quad (2)$$

where,  $v_{50}$  is the ballistic limit. If both sides of Equation (1) are multiplied by the constant, A, and the power 2 is replaced by p, the above equation changes to:

$$v_i^p = Av_r^p - B \quad (3)$$

where, A and B are constant. Equation (3) is known as Lambert-Jonas relations and is used to estimate the ballistic limit in the work. In order to obtain A and B, the experimental impact-residual velocities curve is produced using a curve fitting technique for various values of the power, p. The horizontal and the vertical axes of the graph are assigned to the impact and residual velocities, respectively. The value of the impact velocity at the point where the fitted curve intersects with the horizontal axis defines the ballistic limit which is shown by  $v_{50}$ . Equation (3) is frequently used for determining the ballistic limits of materials [17, 18]. The ballistic limit may be affected by the geometry of projectile and the target [19, 20] and also by heat treatment of the material [21]. The effects of the projectile tip shape and mass and target thickness on the ballistic limit of the material are also investigated in this work. Furthermore, the effect of quenching on the ballistic limit of the material is studied.

## 2. MATERIAL AND SPECIMEN

The high strength low carbon alloy, known as HSLA-100 has been used in this investigation. The chemical composition of the material as obtained from spectrometry analysis is shown in Table 1. The wt% of the elements of the material shown in Table 1 conforms to the standard composition of HSLA-100 [22, 23]. In the current study, HSLA-100 steel was used in the form of as-received and quenched samples. A number of specimens were heated up to 950°C for 40 minutes, were quenched in water and then were cooled in air [13]. The stress-strain curves of the as-received and the quenched specimens were obtained by tensile test. The tensile specimens were made according to the standard ASTM-E8. The corrected true stress-strain curves of the materials are illustrated in Figure 1. The correction of the curves was performed using Bridgman correction method [24]. As the figure indicates, the quenching of the material has caused the yield stress to increase from 870 MPa to about 1100 MPa, the ultimate strength to increase from 1470 MPa to about 1700 MPa and the elongation to reduce from 1.2 to 0.74.

The rectangular specimens with 3 mm thickness and 90 mm width were prepared for ballistic tests. The tests were conducted using blunt-ends cylindrical projectiles made of high strength VCN150 steel. The projectiles were heat treated to improve their hardness. A typical projectile is depicted in Figure 2. As the figure shows, the specimens are mounted in a sabot made of polyethylene polymer to decrease the friction and wear between the launch tube and the projectile.

## 3. TEST APPARATUS

Quasi-static tests were conducted on an Instron testing machine. Ballistic tests were carried out using a gas gun. The gas gun was able to launch the projectiles of 10 g at the velocities up to several hundred m/s. The gas gun was equipped with a fixture for holding the specimens (see Figure 3) and the speed sensors to measure the impact and residual velocities (see Figure 4).

**TABLE 1.** Chemical composition of HSLA-100 used in this work

Cr	S	P	Mn	Si	C	Ti
0.56	0.006	0.007	0.83	0.26	0.06	0.003
W	V	Cu	Mo	Ni	Sb	As
0.02	0.003	1.6	0.60	3.85	Trace	0.004
Pb	Sn	Al	Co	Nb	Zr	Fe
0.003	0.005	0.021	0.01	0.03	0.003	Base

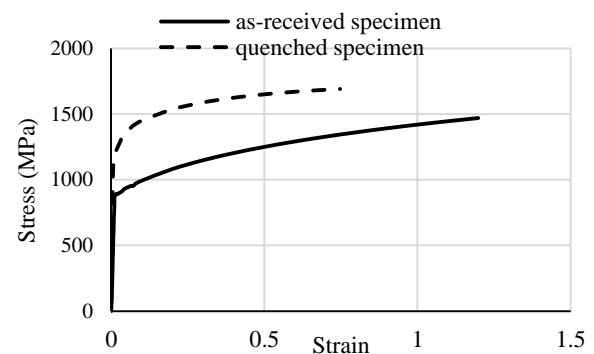


**Figure 1.** The corrected true stress-strain curves of the as-received and the quenched materials



**Figure 2.** The assembly of the projectile and the sabot

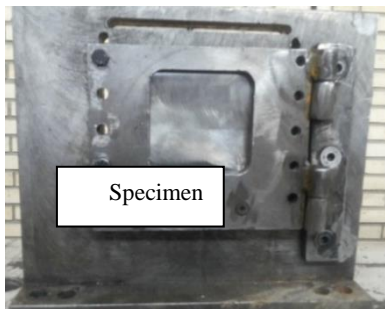


Figure 3. The fixture for holding the specimens



Figure 4. The speed sensors and the fixture

The design of fixture allowed to create built in and simple supports for the specimens. Also, having a hinged door made the quick set up of the specimen possible for ballistic test. It must be mentioned that the specimens were cooled down in a cooling media separately and then were transferred to the fixture for testing.

**4. TEST PROCEDURE**

The experiments consisted of (i) quasi-static tensile tests to characterize the mechanical properties of the as-received and the quenched specimens, (ii) cooling down the specimens and (iii) ballistic tests. The results of the quasi-static tests were presented in section 2. The ballistic tests were performed at 4 four temperatures of ambient temperature, -40, -80 and -196°C. For the sub-zero temperature tests three different cooling chambers were designed. In all three cooling techniques attempts were made to produce a cooling chamber with a stable temperature and to expose the specimens to the cooling temperature for adequate time to make sure that the specimens has homogenously been cooled down.

(i) For -40 °C tests, a mixture of methanol and dry ice was employed. The high thermal capacity of methanol allowed the dry ice to keep the cooling chamber in a stable condition. The temperature rise can be compensated by adding enough ice to the mixture during the process of cooling.

(ii) For -80°C tests, we used dry ice which keeps the temperature constant during process of cooling. The only problem with dry ice was its reduction due to vaporization. Similar to the previous case, the reduction of the ice was compensated by adding enough ice to the cooling chamber during the process of cooling.

(iii) For -196°C, we used liquid nitrogen.

In all three cooling techniques, the specimens were put in the cooling chamber for 40 minutes which was found to be enough to reach a constant temperature throughout the samples.

**5. BALLISTIC TEST RESULTS**

The ballistic tests were performed on the as-received and the quenched materials. For each temperature, six tests at six different velocities were carried out and the impact and the residual velocities were measured. The experimental variation of the residual velocity versus the impact velocity was fitted into a curve using the Lambert-Jonas model for the powers 1.5, 1.75, 2 and 2.25. Finally, the ballistic limit of the material was obtained using Equation (3).

**5. 1. Ballistic Limit of the As-received Specimens**

The impact and residual velocities of the as-received material at ambient temperature are given in Table 2. Lambert-Jonas curve for the as-received material at ambient temperature, -40, -80 and -196°C are illustrated in Figures 5 to 8, respectively.

**TABLE 2.** The impact and residual velocity for the as-received material at ambient temperature

$V_i$ (m/s)	$V_r$ (m/s)
147.6	0
293.8	185.2
315.8	180.0
337.7	209.1
376.6	251.0
404.4	270.0

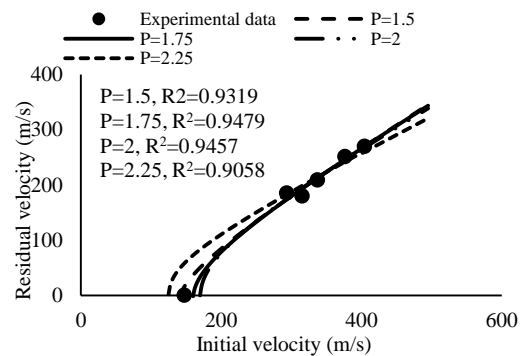
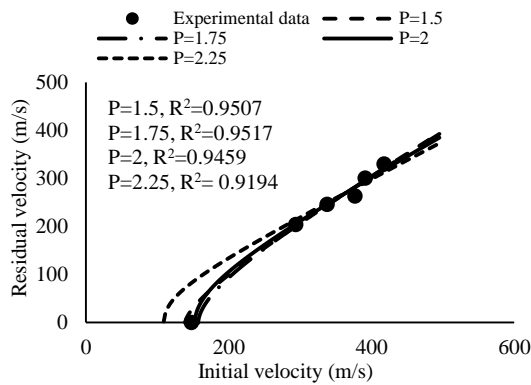
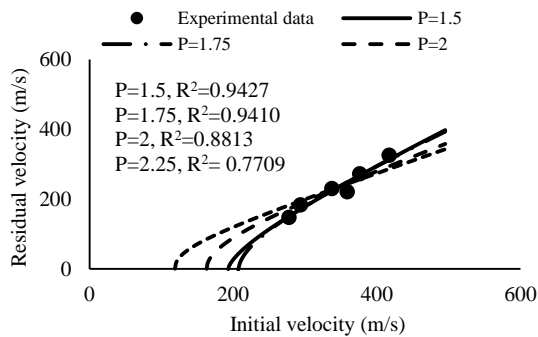


Figure 5. Lambert-Jonas curve for as-received material at ambient temperature

From these figures, the ballistic limit was obtained. The results are provided in Table 3. Variation of ballistic limit versus temperature for various LJ power is shown in Figure 9. As Table 3 and Figure 9 suggest, the ballistic limit does not vary significantly from ambient temperature to  $-40^{\circ}\text{C}$ . However, for the lower temperatures ballistic limit reduces considerably. The increase in ballistic limit for different temperatures with respect to ambient temperature is illustrated in Figure 10. As it is observed, the ballistic limit increases by about 30% and 40% for the temperatures of  $-40$  and  $-80^{\circ}\text{C}$ , respectively.



**Figure 6.** Lambert-Jonas curve for as-received material at the temperature of  $-40^{\circ}\text{C}$



**Figure 7.** Lambert-Jonas curve for as-received material at the temperature of  $-80^{\circ}\text{C}$

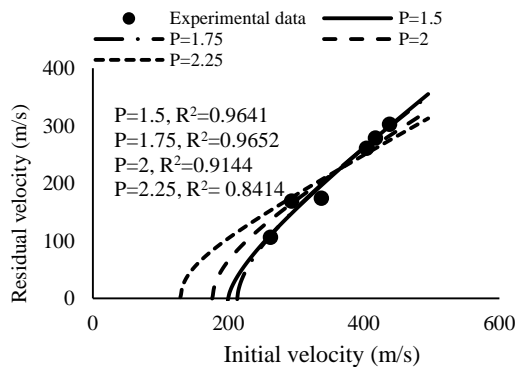


**Figure 8.** Lambert-Jonas curve for as-received material at the temperature of  $-196^{\circ}\text{C}$

**TABLE 3.** Ballistic limits for the as-received material

P	$V_{50}$ (m/s)
Room temperature	
1.5	142.5
1.75	160.7
2	166.0
2.25	103.5
$T=-40^{\circ}\text{C}$	
1.5	139.0
1.75	157.4
2	152.7
2.25	109.6
$T=-80^{\circ}\text{C}$	
1.5	193.1
1.75	207.6
2	163.0
2.25	119.0
$T=-196^{\circ}\text{C}$	
1.5	199.8
1.75	223.3
2	176.8
2.25	154.0

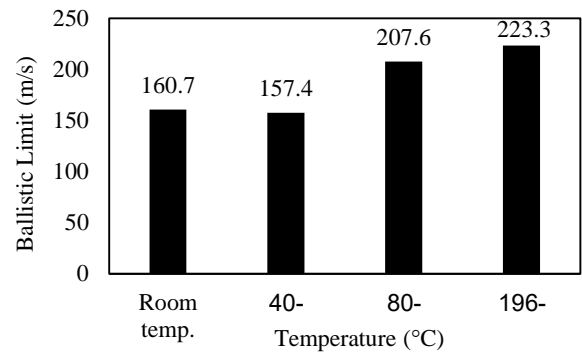


**Figure 9.** Variation of ballistic limit versus temperature for the as received material

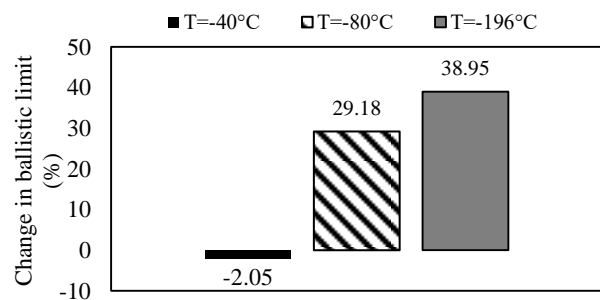


**Figure 10.** The increase in ballistic limit for different temperatures with respect to ambient temperature

**5. 2. Ballistic Limit of the Quenched Specimens**

Lambert-Jonas curve for quenched material at ambient temperature is illustrated in Figure 11. Similar curves can be shown for -40, -80 and -196°C. From these figures, the ballistic limit was obtained. The results are provided in Table 4. As Table 4 suggests, the ballistic limit did not vary significantly from ambient temperature to -40°C. However, for the lower temperatures ballistic limit reduced considerably. The increase in ballistic limit for different temperatures with respect to ambient temperature is depicted in Figure 12.

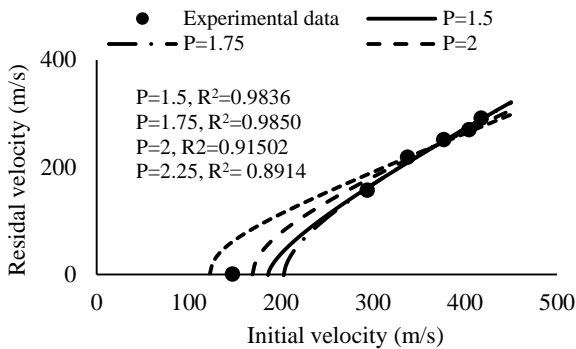


**Figure 11.** Lambert-Jonas curve for the quenched material at room temperature

**TABLE 4.** Ballistic limits for the quenched material

P	V <sub>50</sub> (m/s)
Room temperature	
1.5	186.2
1.75	203.5
2	169.8
2.25	123.5
Temperature=-40°C	
1.5	181.1
1.75	196.9
2	161.0
2.25	118.2
Temperature=-80°C	
1.5	228.2
1.75	238.1
2	165.4
2.25	120.2
Temperature=-196°C	
1.5	260.6
1.75	266.8
2	215.6

As it is observed, the ballistic limit increased by about 15% and 30% for the temperatures of -40 and -80°C, respectively.

The results indicated that the increase in ballistic limit for the quenched specimens was less than that for the as-received materials. The increase in ballistic limit for the quenched material with respect to the as-received specimens is shown in Figures 13 and 14.

**6. NUMERICAL SIMULATIONS**

It is obvious that ballistic limit of a material depends on the material’s properties and geometry particularly the thickness and the projectile geometry specifically its tip shape.

The results provided in section 5 were obtained for 3 mm thick plates impacted by blunt projectile with a 6 mm diameter. In this section, the effect of the specimen thickness and the projectile mass and tip shape on the ballistic limit is studied by numerical simulation. The simulations are also validated by experiment. The validated model is then employed to predict the ballistic limit for different test conditions. The simulations are performed using the well-known hydrocode, Ls-dyna.

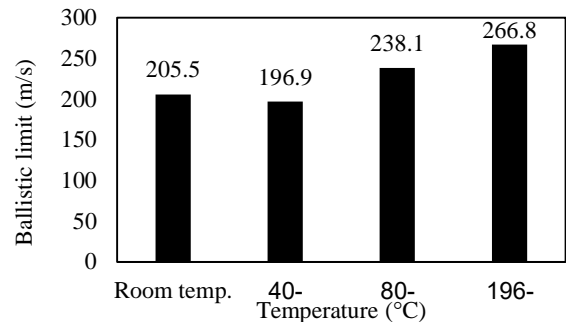


**Figure 12.** Variation of ballistic limit versus temperature for the quenched material

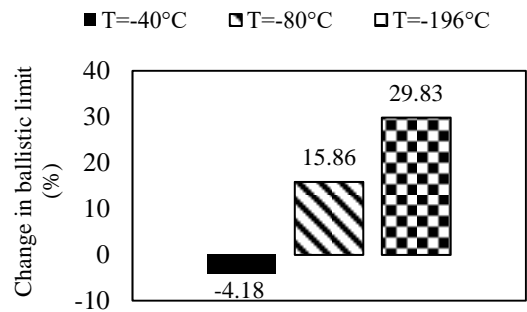


**Figure 13.** The increase in ballistic limit for different temperatures with respect to ambient temperature for the quenched material

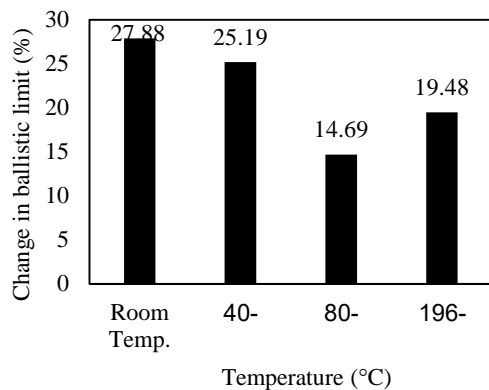


**Figure 14.** The increase in ballistic limit for the quenched material with respect to the as-received specimens.

**6. 1. Numerical Modeling** The numerical model as shown in Figure 15, consisted of the specimen and the projectile. A three-dimensional analysis was employed for the solution of the problem. The simulations converged for 79200 and 972 solid elements for the specimen and the projectile, respectively.

The projectile was assumed rigid and the behavior of the specimen was defined by Johnson-Cook material model. The contact surface was modeled by 3D\_ERODING\_SURFACE\_TO\_SURFACE elements. The constants of Johnson-Cook model were determined from quasi-static tensile tests using an Instron testing machine and dynamic tensile tests using a Split Hopkinson Bar apparatus. The results are given in Table 6.

Mat\_Add\_Erosion was used for damage evaluation. According to this criterion, a damaged element is removed from the model when stress or strain exceeds a pre-defined level. Gruneizen equation of state is used in the simulations. The constants of the equation are given in Table 7.

**6. 2. Validation of Numerical Simulations** The numerical simulations were performed for the as-received material at six velocities used in the experiments. The results are compared in Table 8. It is seen that for the velocity of 147.6 m/s the projectile did not penetrate the target. This was confirmed by both the experiment and the simulation.

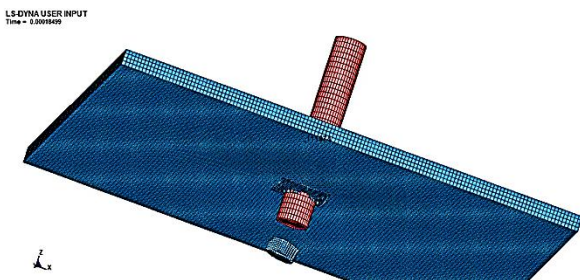


**Figure 15.** Finite element model of the ballistic test assembly

**TABLE 6.** The constants of Johnson-Cook model used in the simulations

A	B	n	c
820	620	0.48	0.15

**TABLE 7.** The constants of Gruneizen equation of state

C (m/s)	S <sub>1</sub>	S <sub>2</sub>	S <sub>3</sub>	γ <sub>0</sub>	A	Initial internal energy	Initial relative volume
5400	1.586	0	0	2.17	0	0	1

**TABLE 8.** A comparison between the experimental and numerical residual velocities

V <sub>i</sub>	V <sub>r</sub> (FEM)	V <sub>r</sub> (Exp.)	Error (%)
147.6	0	0	0
293.8	176.4	185.2	-4.7%
315.8	204.6	180	13.6%
337.7	226.7	209.1	8.4%
376.6	262.4	251.2	4.4%
404.4	308.8	270.6	14.1%

As Table 8 suggests, the difference between the experiments and the simulations is not as significant. The error varies between 4.4% and 14.1%. Variation of the specimen's mass versus time predicted by simulation is depicted in Figure 16. From the figure, the reduction in the specimen's mass can be calculated as 6.7 g. The mass of the fragment of the specimen which was cut out by the projectile after perforating the specimen (shown in Figure 16), obtained from the experiment, was 0.65g. This gives an error of about 3% which is quite acceptable.

### 6. 3. Numerical Results

Similar to the experiments, the residual velocities were obtained from the numerical simulations for the six impact velocities used in the ballistic tests and the Lambert-Jonas curves were obtained for the LJ powers mentioned above. The LJ curves are illustrated in Figure 17.

The ballistic limit was obtained from the figure. The experimental and numerical ballistic limits are compared with each other in Table 9. As the Table suggests, the minimum difference is obtained for the power of 2.

**6. 3. 1 The Effect of Projectile Tip Shape** Three different tip shapes including blunt, conical and hemispherical (oval) were studied in this work. The residual velocities obtained for blunt and oval nose shapes are compared in Table 10. As the Table indicates, the maximum difference is about 16% which is not as significant.

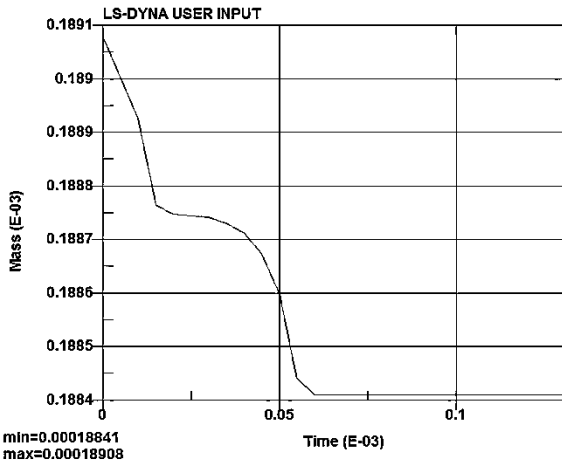


Figure 16. Variation of specimen mass versus time (mass is in ton and time in seconds)

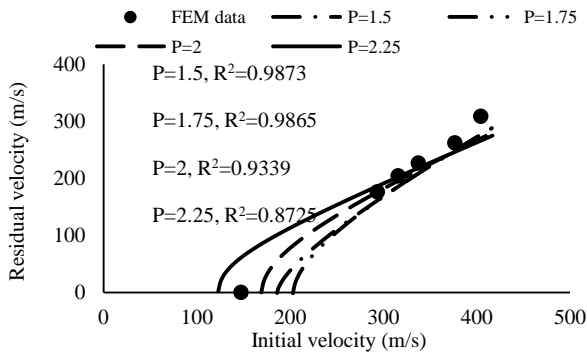


Figure 17. Lambert-Jonas curve for as-received material at ambient temperature

TABLE 9. A comparison between the experimental and numerical ballistic limits

P	V <sub>50</sub> (FEM)	V <sub>50</sub> (Exp.)	Error
1.5	187.2	142.5	31.4%
1.75	203.5	160.7	26.7%
2	160.9	166.6	-3.4%
2.25	117.2	103.5	13.2%

TABLE 10. A comparison between the residual velocities obtained for blunt and oval nose shape

V <sub>i</sub>	V <sub>r</sub> (Blunt)	V <sub>r</sub> (Hemispherical)	Difference
147.6	0	0	0
293.8	176.4	185.2	5.0%
315.8	204.6	235.9	15.3%
337.7	226.7	264.1	16.5%
376.6	262.4	306.0	16.6%
404.4	308.8	339.1	9.8%

It can be drawn out that the oval nose increases the residual velocity but not very considerably. The residual velocities obtained for blunt and conical nose shapes are compared in Table 11.

As the Table indicates, the maximum difference is about 20% which is not as significant. It is concluded that the conical nose increases the residual velocity but not very considerably. The ballistic limits for blunt, hemispherical and conical nose shapes are compared in Tables 12 and 13. As the Tables suggest, the ballistic limit decrease for both the conical and hemispherical nose shapes but the decreases is not remarkable.

6. 3. 2. The Effect of Target Thickness

In order to study the effect of specimen thickness on ballistic limit, two specimens with 2 mm and 3 mm thickness were modeled for the ballistic test simulation. The ballistic limits for the two specimens are given in Table 14. As the Table indicates, the increase in thickness significantly decreases the residual velocity. However, the increase depends on the impact velocity such that it reduces with the increase of the impact velocity. The ballistic limits for the two thicknesses are compared in Table 15. As it is seen, the increase in ballistic limit is nearly the same for all LJ powers.

TABLE 11. A comparison between the residual velocities obtained for blunt and conical nose shape

V <sub>i</sub>	V <sub>r</sub> (Blunt)	V <sub>r</sub> (Conical)	Difference
147.6	0	0	0
293.8	176.4	198.7	12.6%
315.8	204.6	245.5	20.0%
337.7	226.7	272.7	20.3%
376.6	262.4	317.4	19.0%
404.4	308.8	342.3	10.8%

TABLE 12. A comparison between the ballistic limits for blunt and conical nose shape

P	V <sub>50</sub> (Conical)	V <sub>50</sub> (Blunt)	Difference
1.5	175.7	187.2	-6.1%
1.75	193.2	203.5	-5.1%
2	144.8	160.9	-10.0%
2.25	103.8	117.2	-11.4%

TABLE 13. A comparison between the ballistic limits for blunt and hemispherical nose shape

P	V <sub>50</sub> (Hemispherical)	V <sub>50</sub> (Blunt)	Difference
1.5	177.6	187.2	-5.1%
1.75	195.4	203.5	-3.9%
2	142.1	160.9	-11.7%
2.25	101.6	117.2	-13.3%

**TABLE 14.** A comparison between the residual velocities for the two thicknesses

$V_i$	$V_r(2\text{mm})$	$V_r(3\text{mm})$	Difference
147.6	0	0	0
293.8	248.5	176.4	40.8%
315.8	284.5	204.6	39.0%
337.7	300.3	226.7	32.5%
376.6	349.0	262.4	33.0%
404.4	388.9	308.8	25.9%

**TABLE 15.** A comparison between the ballistic limits for the two thicknesses

P	$V_{50}(2\text{mm})$	$V_{50}(3\text{mm})$	Difference
<b>1.5</b>	139.2	187.2	-25.6%
<b>1.75</b>	158.1	203.5	-22.3%
<b>2</b>	127.2	160.9	-20.9%
<b>2.25</b>	89.9	117.2	-23.3%

**6. 3. 3. The Effect of Projectile Mass** The initial mass of the projectile was 3.95 g. In order to examine the effect of mass on ballistic limit, a projectile with 7.89g was also used in the simulation. The residual velocities for the two projectile masses are given in Table 16. As the Table indicates, for the impact velocity of 147.6 m/s, no penetration occurred for 3.95 g mass projectile while the 7.89 g projectile completely perforated the target. The ballistic limits for the two projectile masses are compared in Table 17. As the Table suggests, the increase of projectile mass diminishes the ballistic limit. The reduction, however, depends strongly on LJ power and varies from 13% to about 29%.

## 6. DISCUSSION

The change of ballistic limit with temperature may be due to two possibilities; the change of microstructure or mechanical properties of the material. It has frequently been reported in the literature that no microstructural change occurs in the material at sub-zero temperatures. Therefore, the first possibility is completely ruled out. In order to examine the effect of temperature on mechanical properties of the materials, a number of specimens were tested at the strain rate of  $1000\text{s}^{-1}$  using a tensile Hopkinson bar and at room temperature, -40, -80 and -196°C. From each test, the tensile stress-strain curve was recorded and the yield and ultimate strength were measured. The results are given in Table 18. As the results indicate, the decrease of temperature gives rise to the increase of yield and strength of the materials. Typical SEM pictures are illustrated in Figure 18.

**TABLE 16.** A comparison between the residual velocities for the projectile masses

$V_i$	$V_r(\text{projectile mass}=3.95\text{gr})$	$V_r(\text{projectile mass}=7.89\text{gr})$	Difference
147.6	0	37.8	-
293.8	176.4	232.4	31.7%
315.8	204.6	255.2	24.7%
337.7	226.7	277.9	22.6%
376.6	262.4	316.8	20.7%
404.4	308.8	344.4	11.5%

**TABLE 17.** A comparison between the ballistic limits for the two projectile masses

P	$V_{50}(\text{projectile mass}=7.89\text{gr})$	$V_{50}(\text{projectile mass}=3.95\text{gr})$	Difference
<b>1.5</b>	133.6	187.2	-28.6%
<b>1.75</b>	138.6	203.5	-31.9%
<b>2</b>	138.9	160.9	-13.7%
<b>2.25</b>	100.8	117.2	-14.0%

**TABLE 18.** Yield and ultimate strength for different test conditions

T	Yield stress (MPa)	Ultimate strength (MPa)
Room Temp.	1500	2000
-40°C	1500	2000
-80°C	1600	2200
-196°C	1900	2600

As the figure suggests, for the room temperature and -40°C, the fracture surface is quite dimpled without any trace of cleavage. Although, the density of dimples is clearly higher for room temperature the ductile fracture mechanism seen for both room temperature and -40°C tests verifies the similarity between the ballistic limits for these two temperatures. The fracture surface for -80°C, as observed in Figure 18(c), is a mixture of dimple and cleavage. The surface for -196°C is completely cleaved and shows a quite brittle fracture mechanism for this temperature.

The rate sensitivity of the ballistic limit depends on the temperature and increases with the decrease of temperature. In fact, the dislocation pile-ups which act as barrier to further movement of dislocations at higher strain rates cause more hardening at sub-zero temperatures so that the fracture mechanism changes from completely ductile at room temperature to fully brittle at -196°C.

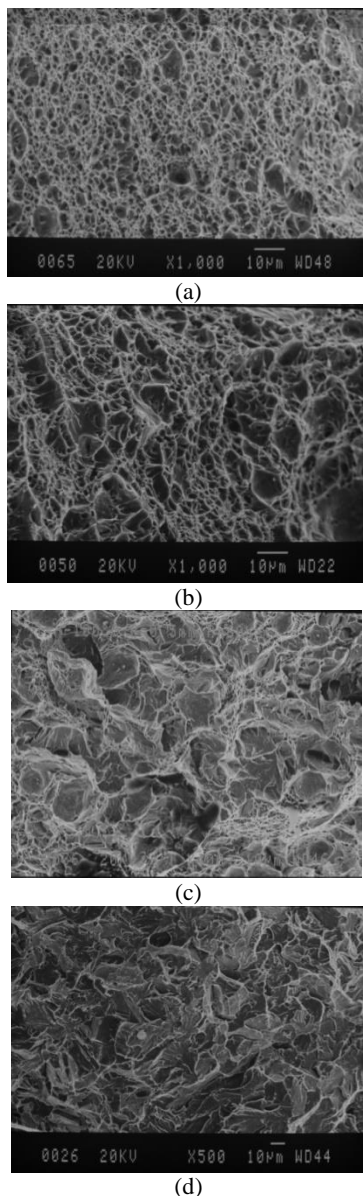


**Figure 18.** SEM pictures of fracture surfaces of the specimens tested in tension (a) Room temperature; (b) -40, (c) -80, and (d) -196°C

## 7. CONCLUSIONS

For the materials tested in this work and the test conditions, the following conclusions may be drawn:

1. For the as-received material, the ballistic limit is nearly the same for ambient and -40°C temperatures, but increases significantly for -80 and -196°C temperatures, respectively.
2. The increase of ballistic limit is lower for the quenched specimens and is 16% and 30% for -80 and -196°C temperatures, respectively.
3. The increase of projectile mass diminishes the ballistic limit.
4. By increasing the thickness of the specimen from 2mm to 3mm, the ballistic limits increased about 20 to 25%.
5. The ballistic limit decreased, for both the conical and hemispherical projectile's nose shapes. The maximum reduction was about 13% for  $p=2.25$ .
6. The fracture mechanism of the materials changed from completely ductile at room temperature to fully brittle at -196°C.

## 8. REFERENCES

1. Holsberg, P., Caplan, I. and Gudas, J., "Navy's welding research picks up steam", *Advanced Materials and Processes*, Vol. 138, No. 1, (1990), 45-46.
2. Thompson, S., Colvin, D. and Krauss, G., "Austenite decomposition during continuous cooling of an HSLA-80 plate steel", *Metallurgical and Materials Transactions A*, Vol. 27, No. 6, (1996), 1557-1571.
3. Palmiere, E., Garcia, C. and DeArdo, A., "Processing, microstructure and properties of microalloyed and other modern hsla steels", *Iron and Steel Society of AIME, Warrendale, PA*, Vol. 113, (1992).
4. Sarkar, A., "A development study of microalloyed steel (HSLA) through experimental exploration", National Institute of Technology Rourkela, (2012),
5. Mattes, V. R., "Microstructure and mechanical properties of HSLA-100 steel", Monterey, California: Naval Postgraduate School, (1990),
6. Das, S.K., Sivaprasad, S., Das, S., Chatterjee, S. and Tarafder, S., "The effect of variation of microstructure on fracture mechanics parameters of HSLA-100 steel", *Materials Science and Engineering: A*, Vol. 431, No. 1, (2006), 68-79.
7. Bhole, S., Nemade, J., Collins, L. and Liu, C., "Effect of nickel and molybdenum additions on weld metal toughness in a submerged arc welded HSLA line-pipe steel", *Journal of Materials Processing Technology*, Vol. 173, No. 1, (2006), 92-100.
8. Xue, Q., Benson, D., Meyers, M., Nesterenko, V. and Olevsky, E., "Constitutive response of welded HSLA 100 steel", *Materials Science and Engineering: A*, Vol. 354, No. 1, (2003), 166-179.
9. Alkhader, M. and Bodelot, L., "Large strain mechanical behavior of HSLA-100 steel over a wide range of strain rates", *Journal of Engineering Materials and Technology*, Vol. 134, No. 1, (2012).
10. Schindler, I., Janosec, M., Mistecky, E., Ruzicka, M., Cizek, L., Dobrzanski, L., Ruzs, S. and Suchanek, P., "Effect of cold rolling and annealing on mechanical properties of HSLA steel", *Archives of Materials Science and Engineering*, Vol. 36, No. 1, (2009), 41-47.
11. Ray, P., Ganguly, R. and Panda, A., "Optimization of mechanical properties of an HSLA-100 steel through control of heat treatment variables", *Materials Science and Engineering: A*, Vol. 346, No. 1, (2003), 122-131.
12. Mujahid, M., Lis, A., Garcia, C. and DeArdo, A., "HSLA-100 steels: Influence of aging heat treatment on microstructure and properties", *Journal of Materials Engineering and Performance*, Vol. 7, No. 2, (1998), 247-257.
13. Dhua, S., Ray, A. and Sarma, D., "Effect of tempering temperatures on the mechanical properties and microstructures of HSLA-100 type copper-bearing steels", *Materials Science and Engineering: A*, Vol. 318, No. 1, (2001), 197-210.

14. Martineau, R. L., Prime, M. B. and Duffey, T., "Penetration of HSLA-100 steel with tungsten carbide spheres at striking velocities between 0.8 and 2.5 km/s", *International Journal of Impact Engineering*, Vol. 30, No. 5, (2004), 505-520.
15. Lambert, J. and Jonas, G., "Towards standardization in terminal ballistics testing: Velocity representation", DTIC Document, (1976).
16. Recht, R. and Ipson, T., "Ballistic perforation dynamics", *Journal of Applied Mechanics*, Vol. 30, No. 3, (1963), 384-390.
17. Nia, A. A., Razavi, S. and Majzoobi, G., "Ballistic limit determination of aluminum honeycombs—experimental study", *Materials Science and Engineering: A*, Vol. 488, No. 1, (2008), 273-280.
18. Kpenyigba, K., Jankowiak, T., Rusinek, A., Pesci, R. and Wang, B., "Effect of projectile nose shape on ballistic resistance of interstitial-free steel sheets", *International Journal of Impact Engineering*, Vol. 79, (2015), 83-94.
19. Jena, P., Mishra, B., RameshBabu, M., Babu, A., Singh, A., Sivakumar, K. and Bhat, T. B., "Effect of heat treatment on mechanical and ballistic properties of a high strength armour steel", *International Journal of Impact Engineering*, Vol. 37, No. 3, (2010), 242-249.
20. Mishra, B., Jena, P., Ramakrishna, B., Madhu, V., Bhat, T. and Gupta, N., "Effect of tempering temperature, plate thickness and presence of holes on ballistic impact behavior and ASB formation of a high strength steel", *International Journal of Impact Engineering*, Vol. 44, (2012), 17-28.
21. Senthil, P. P., Singh, B. B., Kumar, K. S. and Gogia, A., "Effect of heat treatment on ballistic performance of an armour steel against long rod projectile", *International Journal of Impact Engineering*, Vol. 80, (2015), 13-23.
22. Czyryca, E. J., Link, R. E., Wong, R. J., Aylor, D. A., Montem, T. W. and Gudas, J. P., "Development and certification of HSLA-100 steel for naval ship construction", *Naval Engineers Journal*, Vol. 102, No. 3, (1990), 63-82.
23. ASTM A588 / A588M-10, S. S. f. H.-S.L.-A. S. S., "up to 50 ksi [345 MPa] Minimum Yield Point, with Atmospheric Corrosion Resistance", *ASTM International*, West Conshohocken, PA, (2010), [www.astm.org](http://www.astm.org).
24. Bridgman, P. W., "Studies in large plastic flow and fracture with special emphasis on the effects of hydrostatic pressure", *McGraw-Hill*, (1952).

## The Ballistic Behavior of High Strength, Low Alloy-100 Steel at Sub-zero Temperatures

G. Majzoobi, S. Moradi

Mechanical Engineering Department, Bu-Ali Sina University, Hamedan, Iran

P A P E R I N F O

چکیده

### Paper history:

Received 29 December 2015

Received in revised form 29 September 2016

Accepted 30 September 2016

### Keywords:

HSLA-100

Ballistic Limit

Sub-zero Temperature

Lambert-Jonas

Residual Velocity

در این تحقیق، رفتار بالستیک فولاد پر مقاومت و آلیاژ پائین HSLA-100 در دماهای محیط، ۴۰-، ۸۰- و ۱۹۶- درجه سانتی گراد مورد مطالعه قرار می گیرد. معادله لمبرت-جونز برای برازش منحنی های بالستیک مورد استفاده قرار می گیرد. همچنین، تأثیر عملیات حرارتی کوئنچینگ بر رفتار بالستیک فولاد فوق مورد بررسی قرار خواهد گرفت. آزمایش های بالستیک بر روی نمونه های مستطیلی با ضخامت ۳mm و با استفاده از پرتابه های استوانه ای سرتخت انجام می شوند. نتایج به دست آمده نشان می دهند که حد بالستیک برای ماده دریافتی (بدون عملیات حرارتی) در دماهای محیط و ۴۰- درجه سانتی گراد تقریباً یکسان است اما برای دماهای ۸۰- و ۱۹۶- درجه سانتی گراد به ترتیب ۳۰٪ و ۴۰٪ افزایش می یابد. همین نتیجه برای نمونه های کوئنچ شده مشاهده گردید. با این حال، مقدار افزایش حد بالستیک برای نمونه های کوئنچ شده کمتر از نمونه های دریافتی بود و برای دماهای ۸۰- و ۱۹۶- درجه سانتی گراد به ترتیب ۱۶٪ و ۳۰٪ بود. برای بررسی پارامترهای مختلف نظیر ضخامت نمونه، هندسه سر پرتابه و جرم آن بر حد بالستیک فولاد فوق، آزمایش بالستیک با استفاده از نرم افزار Ls-dyna شبیه سازی گردید.

doi: 10.5829/idosi.ije.2016.29.12c.14